PHYSICAL REVIEW B VOLUME 47, NUMBER 13 1 APRIL 1993-I

Molecular-dynamics simulation of stress relaxation on a triangular lattice

Witold Brostow
Center for Materials Characterization and Department of Physics, University of North Texas, Denton, Texas 76203-5308

Josef Kubát
Department of Polymeric Materials, Chalmers University of Technology, 412-96 Gothenburg, Sweden
(Received 2 June 1992; revised manuscript received 29 September 1992)

Simulations were performed using the method of molecular dynamics for ideal lattices and for lattices with defects generated by three different procedures. Curves of relaxation of stress σ vs logarithmic time t were obtained. In agreement with experimental results, the simulated curves exhibit three regions: initial, nearly horizontal, starting at σ_0; central, descending approximately linearly; and final, corresponding to the internal stress σ_i as defined by Li. The existence of the central linear part has been predicted by a cooperative theory. In agreement with the theory, the slope of the simulated central part is proportional to the initial effective stress $\sigma_0^* = \sigma_0 - \sigma_i$. The central part extends over approximately one decade of $\log_{10} t$ for ideal lattices but over several decades for lattices with defects. High values of the imposed strain ε correspond to low internal stresses σ_i, and vice versa. Stress relaxation is mainly due to deformations that occur in the vicinity of the defects, hence the process is related to the defect concentration and the amount of free volume v^f. Collective response of atoms in groups is observed. The origin of the defects does not seem to influence the relaxation.

I. INTRODUCTION AND SCOPE

Service performance and service life of non-fully-elastic materials and components can in general be predicted from the knowledge of dependence of viscoelastic properties with time t. There are two fundamental kinds of transient experiments for such materials, stress relaxation and creep.[1,2] In the stress relaxation mode one determines the time decay of stress, $\sigma = \sigma(t)$, at a constant strain ε; in creep the opposite occurs. The time-temperature superposition principle and shift factors computed by applying that principle make possible the prediction of long-term behavior of viscoelastic materials from short-term tests. Already in 1965 one of us[3] had demonstrated the existence of common features of stress relaxation curves for ostensibly vastly different materials, including a number of metals and polymers. Subsequent experimental studies over the years have confirmed this.[4,5] A theory was developed to account for these features;[6–10] the theory is not specific to any particular class of materials; it is summarized in Sec. II. The objective of the present work is the acquisition of greater understanding of the stress relaxation phenomenon from computer simulations of metal-like lattices and confrontation of the simulation results with predictions of the theory and with experimental findings.

In general, there is a choice between Monte Carlo (MC) and molecular dynamics (MD) simulations. As reviewed by Binder,[11] MC simulations are particularly useful for dealing with phase transitions and related phenomena. MC and MD, as tools to study materials subjected to external mechanical forces, particularly polymeric ones, were compared and discussed in some detail in Ref. 12. Mechanical behavior is mostly simulated by MD, largely dealing with uniaxial tensile forces so as to elucidate the physical significance of the stress-strain curves. An example is a study of ideal solids by Wang *et al.*[13] They found that there is a critical value of the applied stress above which the specimen fails irreversibly via the nucleation of small-scale defects. The stress at failure decreases considerably when the temperature increases.

To our knowledge, stress relaxation in crystals was *not* simulated before. Simulations of plastic deformations in solids were reported in several papers. Thus, Deng, Argon, and Yip[14] simulated atomic glasses under shear stress. They found local, partly dilatant, shear transformations nucleated preferentially in the boundaries of a liquidlike material as the principal mechanism of plastic strain production. The liquidlike material separated small quasiordered domains formed by a well-relaxed glass. Local shear transformations in atomic clusters occurred mostly in the direction of the applied stress. Srolovitz, Vitek, and Egami[15] simulated amorphous metals, showing that regions of inhomogeneous atomic movement, which results in plastic deformation, are not correlated with local-density fluctuations but with regions of high shear stresses. These regions were sustained by the applied stress. Maxima of the radial-distribution function under shear strain were flattened in comparison to the unstrained model.

Since we are also conducting MD simulations of polymers,[16,17] we expect to report stress-relaxation simulation results for polymerlike materials in a later paper.

II. A COOPERATIVE THEORY

The experimental stress relaxation curves, plotted traditionally in $\sigma = \sigma(\log_{10} t)$ coordinates, exhibited three regions: initial, nearly horizontal; a long central region,

descending approximately linearly; and final, corresponding to the internal stress σ_i as defined first for metals by Li,[18] and subsequently found also for polymers.[6,19,20] A number of theoretical models have been developed, aimed at predicting and explaining those curves. Such models have been reviewed in Ref. 21, and their various deficiencies pointed out. Briefly, models that can explain the behavior of metals served poorly for polymers and vice versa; see also Ref. 10. Moreover, the collective response typically was not taken into account.

Because of these problems, a *cooperative* model, which seems to possess sufficient generality, was developed.[6–10] The model assumes a two-level system, with unrelaxed flow units in the upper level. Thus, the number n of such units at any given time serves as the measure of stress σ, or, more accurately, of the difference $\sigma-\sigma_i$. The flow process consisted of elementary events (transitions) of varying multiplicity; that is, the events formed clusters of different sizes. The relaxation of a cluster of size s was assumed as

$$\dot{n}_s = dn_s/dt = -sn_s/\tau \ , \tag{1}$$

where n_s was the number of unrelaxed flow units in clusters of this size and τ a relaxation time for a single event. The clustering mechanism was formally equivalent to the interaction underlying the Bose-Einstein distribution and related to the phonon characteristics of the system disturbances produced by the elementary events. As in that distribution, single events were spontaneous. Each event might produce a number of induced or secondary events. This led to

$$\mu\dot{n}_s = -s/[e^{s/\beta}-1] \ , \tag{2}$$

where μ was a numerical factor; the maximum cluster size at $t=0$ is $\beta=(-6\mu\dot{n}_0)^{1/2}/\pi$, while $\dot{n}_0$ was the total flow rate at $t=0$.

Given the shape of the experimental curves described above, particularly important was the slope

$$F=[d\sigma/d(\ln t)]_{\max} \ . \tag{3}$$

Distribution (2) led eventually[10] to

$$F=n_0/(\ln\beta+\gamma) \ , \tag{4}$$

where γ was the Euler constant. Since the original total number of flow units n_0 within a cooperative region was proportional to the initial effective stress σ_0^* defined as

$$\sigma_0^*=\sigma_0-\sigma_i \ , \tag{5}$$

from (4) we had

$$F=c\sigma_0^* \ . \tag{6}$$

Here c is a proportionality factor, found experimentally to have values near to 0.1 at ambient temperatures for metals, polymers as well as for a number of other solids.[3]

A somewhat more generalized model, which allowed transitions to lower-as well as to higher-energy states[22] led to essentially the same results. Ostensibly, the present model yielded results largely equivalent to those obtained when using the concept of stress-dependent thermal activation (SDTA).[5] For instance, an exponential relation between the rate dn/dt and n was obtained in both cases. However, the cooperative approach made it possible to linearize the process with regard to σ_0^*, as required by Eq. (6). Such a linearization was *not* possible in SDTA because of the assumption of the energy of activation decreasing linearly with the effective stress.

Under these circumstances, an important question is this: Could we execute simulations realistic enough to exhibit the same features as the experiment and the theory, while at the same time providing information on the nature of the transitions postulated by the model? MD simulations had already been found effective in probing processes that were difficult to handle by analytical theories. Thus, valuable insights had been obtained in studies of diffusion kinetics,[23] crystal growth,[24] phase structures and melting,[25–29] including complicated cases of monoatomic materials on graphite.[27–29] Of course, simulations do not replace either theory or experiment. Their unique capability is the reproduction of macroscopic behavior, while structures and interactions are controlled: Interaction potentials are precisely defined, while decisive parameters can be varied one at a time. We expected that these features would be advantageous also in the elucidation of processes which occur during stress relaxation.

III. THE SIMULATION PROCEDURE

Stress relaxation was simulated by MD for a single-component system of particles placed on the two-dimensional triangular lattice. We used this lattice, since all nearest neighbors are equivalent and the respective coordination number $z=6$ also occur in three-dimensional real crystals.

All simulations had been performed for systems interacting via the most popular 6–12 Lennard-Jones potential (based on the pioneering work by Mie[30]), that is

$$U(R)=4u_{\min}[(r_\sigma/r)^{12}-(r_\sigma/r)^6] \ ;$$

here r_σ is the collision diameter, so that $U(r_\sigma)=0$, while for the minimum of the potential we have $R_{\min}=2^{1/6}r_\sigma$. We defined the reduced units of length $\tilde{R}=R/r_\sigma$. Other reduced units are the same as defined by Allen and Tildesley;[31] in particular, the reduced energy is $\tilde{U}=U/u_{\min}$, the reduced time $\tilde{t}=t[u_{\min}/(mr_\sigma^2)]^{1/2}$ and the reduced temperature $\tilde{T}=k_BT/u_{\min}$, where k_B is the Boltzmann constant. Forces and stresses are measured, respectively, in units of $u_{\min}/r_\sigma$ and $u_{\min}/r_\sigma^2$. Since all particles have equal mass, for perspicuity we have taken that mass as the mass unit: $m_i=1$. Conversion into realistic metal parameters can be achieved[13] by taking $u_{\min}=2.5\times10^{-20}J$ and $r_\sigma=0.25$ nm.

In our simulations an N-particle system was placed in a cell with periodic boundary conditions. We used a MD technique that allowed the simulation cell to change size and orientation in response to any imbalance between internal and external stresses, as well as provide control of the temperature of the system. Among various methods of doing this[31] we chose a procedure of Berendsen *et al.*[32] It was noted by Brown and Clarke[33]

that in this method the motions of the cell were damped to such an extent that the danger of unphysical oscillatory response to changes in the applied stress is practically eliminated. Thus, this seemed to be a preferred method for simulation of nonequilibrium properties of condensed phase systems. Moreover, the method turned out to be relatively easy to implement.

The cutoff radius used in simulations was taken as $r_{\rm cut}=2.5R_{\rm min}$; that is, first and second neighbors were taken into account. We have found that using higher cutoff radii did not change the course of the simulations and had no effect on the results. During the simulations, at the beginning of each time step, the velocities $\mathbf{v}_i(t)$ were updated for each particle as follows:

$$\mathbf{v}_i(t+\Delta t/2)=\mathbf{v}_i(t-\Delta t/2)+\frac{\mathbf{F}_i(t)}{m_i}\Delta t \ . \tag{7}$$

Here Δt is the time step, $\mathbf{F}_i(t)$ the force acting on ith particle, and m_i is the respective particle mass. We have taken $\Delta t=0.0075$; in the remainder of this paper, unless indicated otherwise, we shall use the reduced variables as defined above, but from now on we shall *drop* the tildes.

The system temperature was defined in terms of the particle average kinetic energy. To maintain the system at a particular temperature, the particle velocities obtained from Eq. (7) were rescaled:

$$\mathbf{v}_i'(t+\Delta t/2)=\lambda(t+\Delta t/2)\mathbf{v}_i(t+\Delta t/2) \ , \tag{8}$$

where the coefficient $\lambda(t)$ is given by

$$\lambda(t)=(1+\kappa_T[T_0/T(t)-1])^{1/2} \ . \tag{9}$$

κ_T is the rate of thermal relaxation, which defines the strength of coupling between the system and a "thermal bath." We use $\kappa_T=0.05$ so that the coupling is sufficiently weak. T_0 is the reference temperature. The temperature of the system T was obtained from the kinetic energy E_k; since our systems were two-dimensional, using our reduced temperature we had $E_k=Nu_{\rm min}T$. The kinetic energy was calculated by the summation of squared velocities over all particles:

$$E_k(t)=\tfrac{1}{2}\sum_{i=1}^{N} m_i v_i^2(t) \ . \tag{10}$$

Updated coordinates of the particles $\mathbf{r}_i(t)$ were computed as

$$\mathbf{r}_i(t+\Delta t)=\mathbf{r}_i(t)+\mathbf{v}_i'(t+\Delta t/2)\Delta t \ . \tag{11}$$

Then the periodic boundary conditions were applied to the particle coordinates. These coordinates—and the coordinates of the simulation cell as well—were scaled as follows:

$$\mathbf{r}_i'(t+\Delta t)=\{\underline{1}+\kappa_\sigma[\underline{\sigma}_I(t)+\underline{\sigma}_E(t)]\}\mathbf{r}_i(t+\Delta t) \ . \tag{12}$$

Here $\underline{1}$ is the unit tensor, and $\underline{\sigma}_I(t)$ and $\underline{\sigma}_E(t)$ are, respectively, the tensors of the internal and external stress. We used a convention such that in tension the external stress imposed on the material was positive, while the internal stress induced in the sample was negative. To balance the tension, these two stresses had to have opposite directions. The coefficient κ_σ describes the strength of the coupling between the unbalanced stress and the size of the cell. We present below results for $\kappa_\sigma=0.0005$. However, we checked that the systems behave very similarly for values of $\kappa_\sigma=0.0004$ and 0.000 625. We also found that for values of κ_σ twice as large—or twice as small—as 0.0005, the cell became unstable and collapsed.

The internal stress tensor is given by

$$\underline{\sigma}_I(t)=\frac{1}{V}\left[\sum_{i=1}^{N} m_i\mathbf{v}_i\mathbf{v}_i-\sum_{i=1}^{N-1}\sum_{j=i+1}^{N}\mathbf{r}_{ij}\mathbf{F}_{ij}\right] , \tag{13}$$

where $\mathbf{r}_{ij}$ is the vector difference $\mathbf{r}_i-\mathbf{r}_j$ evaluated using the periodic boundary conditions,[34] while $\mathbf{F}_{ij}$ is the force acting on the ith particle from the jth particle; V is the volume (that is, the area in the two-dimensional system) of the simulation cell. Since the cutoff radius defined above was used, not all pairs were actually taken into account in the summation.

In a typical stress relaxation experiment at room temperature the time span is 10^5–10^7s. Spending that much real time on a computer is impractical. Moreover, and more importantly, the computer samples were much smaller than specimens studied in experiments, so our samples should have responded much faster; this point was discussed in earlier modeling of stress-strain curves.[17] We ascertained, however, that the size of the system studied did not affect the simulation results; see below the beginning of Sec. V. Calculated stress was averaged over 2000 time steps.

To be sure that we were well inside the solid state during stress relaxation, we approximately determined the melting transition by stepwise increase in the temperature under a low pressure. The onset of melting was observed above the reduced temperature of 0.41, while accurate simulations of melting in such a system by Abraham[25,26] located the melting point as $T_m=0.45$, with the onset of the process somewhat below T_m. His results showed that the system was fully stable at $T=0.40$. We find this also for our system: The curve of the kinetic energy E_k as a function of time t at $T=0.40$ shown in Fig. 1 exhibits

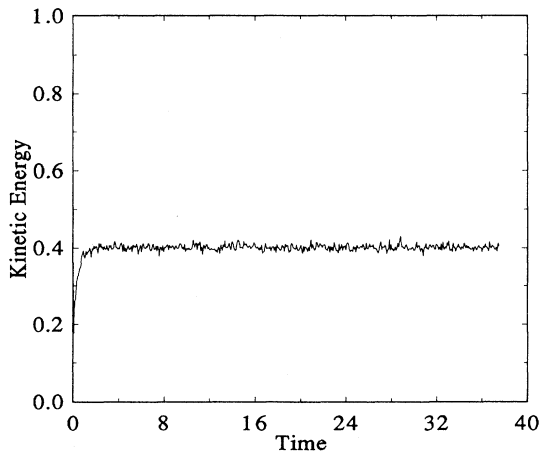

FIG. 1. The kinetic energy vs reduced time at the reduced temperature $T=0.4$.

only random and insignificant fluctuations, and analogous curves for $T=0.1$ and 0.2 look quite similar. Our subsequent stress relaxation simulations were performed at temperatures between 0.1 and 0.4.

The concept of competition between chain relaxation capability (CRC) and destructive processes in viscoelastic materials was developed[35] and resulted in deriving quantitative relationships involving the brittle-ductile impact transition temperature, rapid crack propagation, slow crack propagation, and a connection between isobaric expansivity and dynamic-mechanical behavior; for a review see Ref. 36. While a quantitative measure of CRC of the material needs to be defined for each specific process, such measures are, in general, related to free volume v^f. The latter can be defined by

$$v=v^*+v^f , \tag{14}$$

where v is the specific volume per unit mass such as 1 g, while v^* is the characteristic ("hard-core, incompressible") volume. One often uses instead

$$\tilde{v}=v/v^* . \tag{15}$$

In turn, v^f (or $\tilde{v}$) is related to the isobaric expansivity $\alpha=V^{-1}(\partial V/\partial T)_p$. A statistical-mechanical theory developed by Flory[37,38] leads to the formula

$$\tilde{v}=\{\alpha T/[3(1+\alpha T)]+1\}^3 . \tag{16}$$

However, it is useful to consider more than just two components of the specific volume;[39–41] specifically

$$v=v_W+v_n+v_i+v_d , \tag{17}$$

where v_W is the proper volume of the atoms, calculable from their van der Waals radii; v_n is the nonaccessible volume between atoms, in principle calculable also from the radii and from the interatomic distances; v_i is the volume involved in vibrations of atoms or other particles (ions, polymer segments), also known as the bound or attached volume; and v_d is the detached volume (independent holes). Neutron-scattering studies showed[42] that the frequency of vibrations did not change with the temperature T, but the amplitude did. v^* can be approximately identified with v_W+v_n. The amount of bound volume v_i that can be attached to a particle seems to have an upper limit.[43] We saw that Eqs. (15) and (16) take into account predominantly bound free volume rather than independent holes (i.e., lattice defects), although the volume of the latter also changes with the temperature. We needed to calculate for our computer-generated samples the free volume created by temperature changes, as reflected by α in Eq. (16). At each temperature, the horizontal width of the sample was calculated as $\Delta I_x=x_2-x_1$, where x_1 is the average coordinate of atoms in the vertical left outside row and x_2 a similar coordinate for the right outermost row. Analogously, ΔI_y was evaluated as the difference in the vertical coordinates of the top and bottom rows of atoms. The temperature increase of the lattice parameter averaged over x and y directions was used as the measure of α in Eq. (16), the two-dimensional reduced volume $\tilde{v}^{2/3}$ calculated therefrom, and then two-dimensional v^* and v^f obtained from Eqs. (15) and (14).

Any of the systems obtained as described in the following section were first equilibrated in two stages: at $T=0.4$ for $5000\Delta t$ and then at a temperature somewhat lower than that foreseen for stress relaxation for $25000\Delta t$. Although the initial configuration is constructed on a lattice with the interatomic distances of $R_{\min}$, the equilibration procedure ensured that the configuration was appropriate for the off-lattice MD simulations. Then in each case uniaxial stresses were applied instantaneously along the y axis. We performed most simulations at high strains, often at 10% strain.

IV. SAMPLE PREPARATION

We did not know *a priori* to what extent the ideality of the lattice—or lack of it—affects the spectrum. Therefore, we performed four series of simulations: first for ideal lattices and then for lattices with defects deliberately introduced by three different procedures. We wanted to see whether the origin of the defects affects the results.

In the first procedure, the defects were generated on the computer by melting of the two-dimensional crystal lattice and subsequent quenching. A constant volume was maintained. Temperature was varied in steps that ranged from 0.025 to 0.1. For restoring the thermal equilibrium during quenching, each temperature reduction was followed by 10^3 time steps of stabilization.

The second algorithm of defect generation was based on the fact that undercooled samples generated under an external pressure are more stable than those obtained in the absence of such pressure—as found in the MD simulations of Deng, Argon, and Yip.[44] For high quenching rates and pressures $P>0$ the intensive properties (configurational energy U^c, enthalpy H, or volume V) decrease continuously and monotonically. Then the melting and freezing curves might not meet at all below the melting temperature T_m. However, for $P=0$ the material, even if undercooled at tremendously high quenching rates, was unstable and could undergo crystallization. In fact, in some of our samples generated by the first method, crystallization did occur on quenching, causing disappearance of the majority of the defects. Of course, spontaneous crystallization of an undercooled material represents one more common feature of real and of our simulated materials. The problem of maintaining a predefined external pressure was dealt with by Andersen[45] and by Parinello and Rahman.[46] The shape and size of the simulation cell could be varied as a function of any imbalance between the internal stress and the predefined external pressure. We followed the procedure of Parinello and Rahman and generated a lattice with defects under various pressures $P>0$. The samples so obtained were stable and contained sufficient concentrations of defects.

In the third procedure one started again with the perfect lattice, with all the lattice sites occupied, and then generated vacancies. Randomly chosen particles were moved from the interior of the sample to an additional layer (or several additional layers if necessary) of the sites located at a side of the cell. For all system sizes, in this

procedure a constant fraction of the number of particles ($N/30$) was always moved, generating a proportionate number of vacancies.

V. RESULTS AND DISCUSSION

We found that MD simulations of stress relaxation required a cuttoff radius such as defined above (with the second-nearest neighbors included), as well as frequent updates of the neighbor table. Only under these conditions were structural changes, occurring during relaxation, stable. When the cutoff radius was such that only the nearest neighbors were taken into account, imposition of the strain did not result in the decrease of the width of the sample in the perpendicular direction. By contrast, when the second-nearest neighbors were included, strain imposition caused the width to decrease, as it occurred in real materials, resulting in values of the Poisson ratio $\nu < \frac{1}{2}$.

Numerical calculations for defective lattices are much more time consuming than for ideal lattices. The size of the system with defects, which can be simulated with reasonable computational effort, was therefore limited to several hundred particles. However, we ascertained that the sizes of the systems studied were such that reliable results were obtained. In Fig. 2 we show results for three systems, generated by the third procedure described in the preceding section, at $T=0.2$. The smallest system shows somewhat larger fluctuations, but—within the size range studied—the shape of the stress relaxation curve is unaffected by the size of the system. Analogous diagrams for $T=0.1$ and 0.3 lead to the same conclusion.

Consider now our results from the series of simulations performed for ideal lattices. We have consistently found here that stress relaxation results mainly from propagation of cracks. The usual mechanism of stress concentration at the crack tips is operative here, as characterized in macroscopic experiments by the stress concentration factor $K_t = 1 + 2(h/l)^{1/2}$, where h is one-half the length of the major axis in a hole assumed elliptical and l the radius of curvature at each end of the major axis (see for instance Ref. 47). In Fig. 3 we present a relaxation curve typical for this series. The lattice structure corresponding to the final approximately horizontal part of the same curve is shown in Fig. 4. We see a considerable number of microcracks of various sizes, oriented approximately (but not quite) along the straining direction. Eventually, crack propagation led to the failure of the lattice. The time span of the relaxation process was relatively small.

It is instructive to compare our results to those of Wang and his colleagues.[13] They also studied ideal lattices and obtained realistic results with positive Poisson ratios. Their curve of the internal restoring force f_1 vs time for the failure-causing external force looks qualitatively similar to our Fig. 3. However, the difference in the type of the mechanical experiment simulated has certain consequences. In their tensile mode, when the applied force is below the failure level, the restoring force fluctuates around a constant level; when the failure level is exceeded, the failure occurs very rapidly. In stress relaxation, we always found a stress lowering with time, with the central part descending at a lower rate than in their catastrophic case. At the same time, we found similarities between the two modes at the atomic level: It appears that in both cases defect generation occurred followed by growth of the defects and eventually crack propagation.

We extensively investigated systems with defects. An example of a defective lattice generated by the partial melting procedure described in Sec. III is presented in Fig. 5. In contrast to Fig. 4, which shows a lattice after relaxation, Fig. 5 shows the lattice "as received," before the imposition of strain. By defects we mean here any deviations from structure regularity such as single vacancies, voids, etc. It is worth noting that the imposition of a hydrostatic pressure decreased the interparticle distance and slowed down the movement of structural elements in the crystal.[48–50] Since by starting stress relaxation we were abruptly increasing that distance, the mobility of the structural elements had to rise rapidly at the

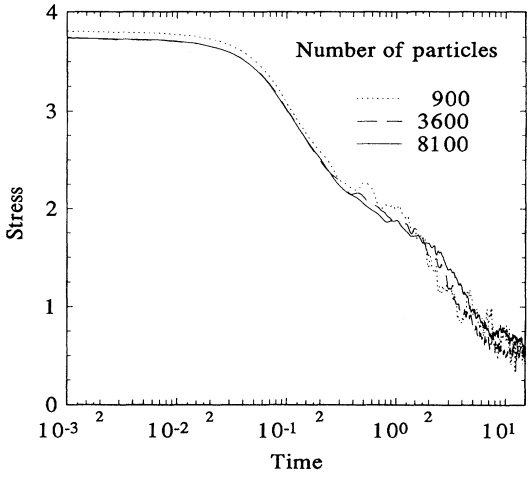

FIG. 2. Stress relaxation curves as a function of log (reduced time) for three metal plus vacancies systems at the reduced temperature $T=0.20$ and the initial strain of 10.0%. The numbers of particles in the central cell are indicated in the inset.

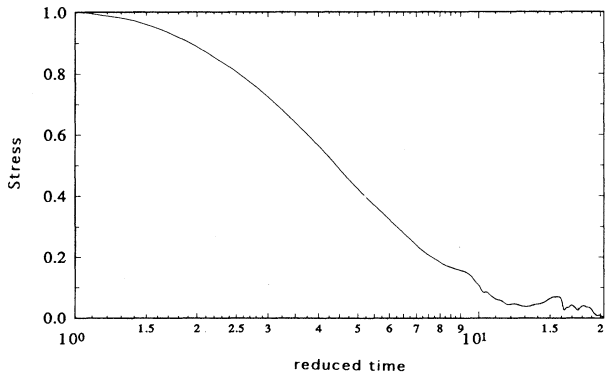

FIG. 3. An example of a stress relaxation curve in the stress vs log (reduced time) coordinates for an ideal (defect-free) lattice; $T=0.31$, a rectangular central cell with 100×150 atoms.

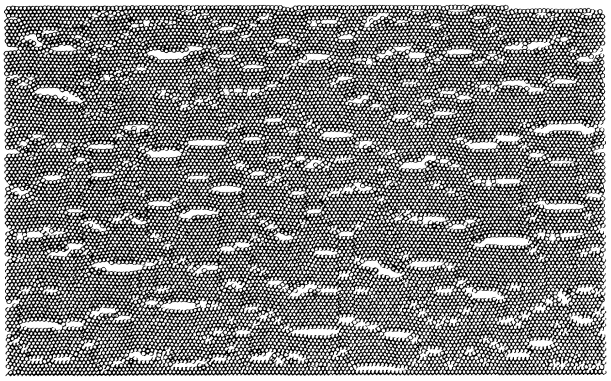

FIG. 4. View of a lattice at the stage of reaching the approximately horizontal part of the stress vs the log time curve when stress $\approx$ internal stress. The original lattice was an ideal one.

same time.

The stress relaxation curve obtained for the lattice in Fig. 5 is shown in Fig. 6. It is apparent from the latter that the time span of relaxation is significantly larger than that for the ideal lattices—this by several orders of magnitude; again see also Fig. 2. We recall that, except for some "degenerate" cases such as whiskers, real metals and other crystalline materials as a rule contain definite concentrations of defects—zero dimensional as well as those of higher dimensionalities including dislocations.[51] Analysis of changes of shape and size of our lattice defects during the simulations showed that the microscopic mechanisms underlying stress relaxation were significantly different from those in lattices without imperfections. We found consistently that stress relaxation is mainly caused by plastic deformations, which occurred in the vicinity of defects. In other words, there was a certain similarity between crystal nucleation from a melt and "nucleation" of cracks. In the ideal lattice, relatively large forces were needed to create a crack, but then the same forces were sufficient for quick propagation. In lattices with defects, relatively small forces caused atomic movements, but the movements were mainly of the ductile or flow type, rather than brittle crack propagation;

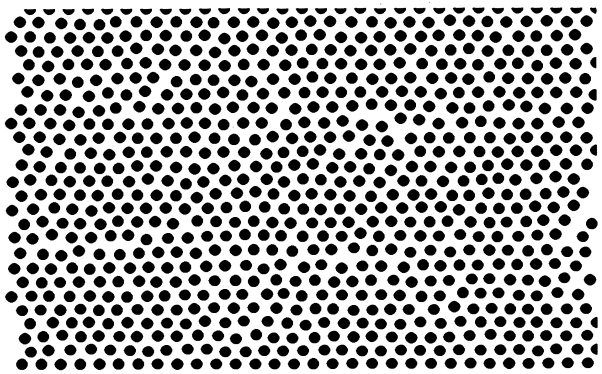

FIG. 5. A major part of a 30×30 atom lattice with defects before strain application.

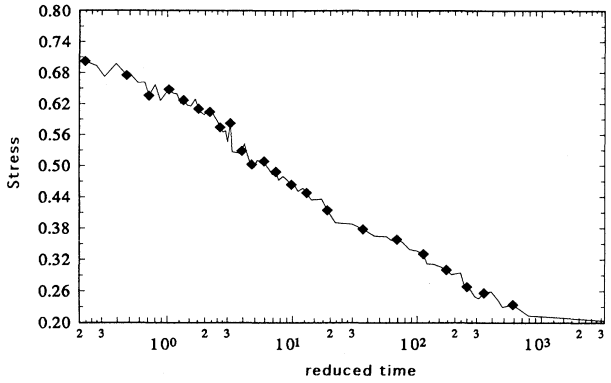

FIG. 6. The stress relaxation curve obtained for the lattice shown in Fig. 5; $T=0.31$.

this is the main factor determining the time span of the relaxation in these two series of simulations.

The deformations we saw resembled the regions of inhomogeneous atomic movement observed by Srolovitz, Vitek, and Egami.[15] While they simulated amorphous metals to obtain stress-strain curves, there were several similarities to the behavior of our crystals during stress relaxation. They observed nucleation of cracklike defects caused by loading, as well as localized viscous flow, and concluded that the material behaves as viscoelastic. They noted that flow is caused by a large number of microscopic deformation events—just as we saw movement of dislocations and other flow units during relaxation. They inferred that there is no single activation barrier for the defect formation but rather a distribution of the activation energies. Such a distribution is predicted by the cooperative theory [Eq. (2)] for stress relaxation as well as observed in our simulations. Moreover, they also concluded that local flows are controlled by multiaxial atomic-level stresses rather than by the applied stress; similarly, we observed movements not necessarily in the direction of the applied strain. An interesting phenomenon, observed in Ref. 15, called mechanical annealing, consists of mutual annihilation of regions with low (n-type) and high (p-type) local density, apparently as a consequence of the stress field assisting the flow of atoms from compressive to tensile regions. This means that the stress field affects the detached free volume v_d [see Eq. (17)] rather than the other way around. By contrast, the bound free volume v_i might be little affected in the mechanical annealing process.

We note that the cooperative theory did predict[5] that "the flow units... during the stress relaxation process... induce transitions of other unrelaxed flow units," exactly as we see every time in our simulations. The necessary condition for obtaining stress relaxation curves similar to the one shown in Fig. 6 is a relatively uniform distribution of defects and the absence of high internal stresses. A similar condition holds for real materials.[3]

In Fig. 7, as in the experimental results,[4] we see a proportionality between the slope of the linearly descending part of the relaxation curve and the initial effective stress σ_0^*. Equation (6) of the cooperative theory predicted the same result, so theory, experiment, and simulation are all

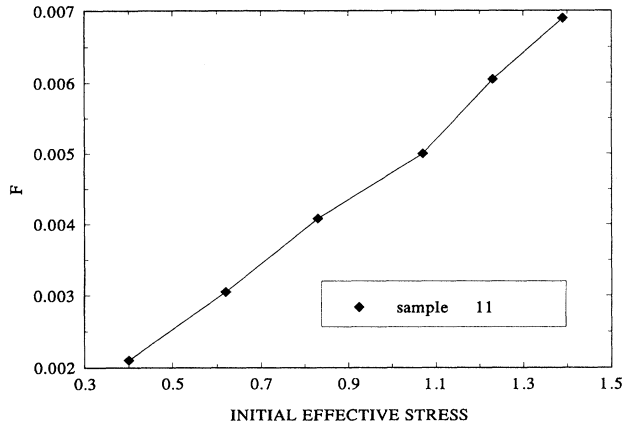

FIG. 7. Slope F of the central (linearly descending) part of the stress relaxation curve plotted as a function of the initial effective stress obtained for a series of simulations of the same sample subjected to different strain levels; $T=0.31$, the central cell of 30×30 atoms.

in agreement. In this case, the bound free volume [Eqs. (15)–(17)] was relatively low, $\approx 1\%$, and $c\sigma_i$ was small. Consequently, a plot of F vs σ_0 is similar to that shown in the figure. One of us pointed out earlier[21] that sometimes one *can get away* with neglecting σ_i. This, however, is not always the case in experiments, and in our simulations as well; see Fig. 8.

As noted above, Eq. (16) takes into account effects of temperature changes upon v^f but does not involve the original concentration of defects. In view of this, we performed a series of simulations for the same sample and subjected to the same strain level but at different temperatures. Two effects of increased T and v^f were observed.

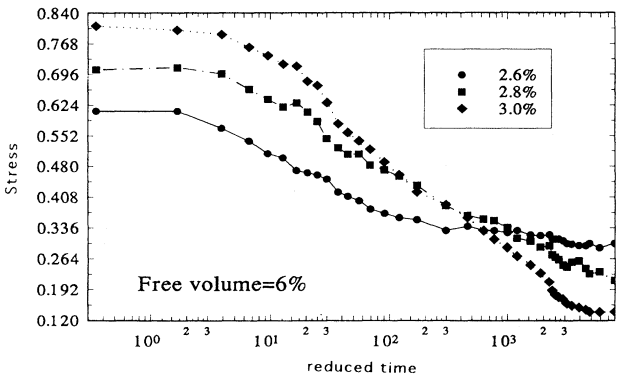

FIG. 8. Three stress relaxation curves for the same sample obtained under constant pressure conditions and with the same free volume but subsequently subjected to different strain levels. Symbols pertaining to strain values in % are indicated in the inset; $T=0.31$, the central cell of 30×30 atoms.

First, the initial stress level σ_0 decreased along with increasing v^f. Second, the time t_i to reach the internal stress level σ_i decreased somewhat with increasing v^f. Both findings are consistent with our earlier understanding of the role of free volume on the atomic and molecular mobility. We recall[52] the results of the Voronoi-Delaunay tessalation of several computer-generated samples: both solidlike (high density, low mobility, nearly regular structure) and liquidlike (low density, high mobility, irregular structure) percolative clusters are possible.

We have also performed stress relaxation simulations for samples with defects prepared by the procedure involving imposition of an external nonzero pressure. We have already shown in Fig. 2 stress curves for systems obtained by random creation of vacancies. In all three series, the results were similar. In other words, the presence of defects affects the results, but the *origin of defects does not.*

Some further results obtained with the procedure involving an external nonzero pressure are shown in Fig. 8. We display three curves, all corresponding to the same v^f, but with different values of the initially imposed strain (inset in the figure). The strain values were relatively high as compared to those imposed in experiments on metals. One infers from the figure that high values of strain ϵ correspond to low values of internal stress σ_i, as well as vice versa. This is readily understandable: Imposition of a higher strain destroys the internal stress to a higher extent. While this is not an unexpected result, once again our simulations provide a verification procedure for concepts developed on the basis of macroscopic experiments.

VI. CONCLUDING REMARKS

Experimental determination of stress relaxation constituted one of the main procedures of prediction of long-time behavior from limited-time testing. It is for this reason that so much attention has been paid to it, and so many approaches describing it have developed. Simulations provide, first of all, insights at the atomic and molecular level into the nature of the phenomenon. At the same time, computer modeling provides the capability of evaluation of the validity of these various approaches and assumptions made in interpreting experimental results.

Lattice systems simulated in this work are, of course, akin to crystalline metals. We found that lattice defects played an important role in stress relaxation. Time scales were affected, as can be seen by comparing Fig. 3 with Figs. 2, 6, and 8; there was an approximate proportionality between the length of the descending part of the curve and the defect concentration. Real crystals are characterized by equilibrium concentrations of defects such as vacancies and methods of calculation of those concentrations exist; see, e.g., Sec. 7.4 in Ref. 51. It is, therefore, not surprising that experimental stress relaxation curves for different materials at comparable temperatures have comparable linear descending parts. Details of each curve depend on the free volume present in the system (as

imposed by the temperature) and on the strain ε via the initial stress σ_0 or, more accurately, via σ_0^*.

It was concluded in the preceding section that the atomic mechanism of stress relaxation involves to a large extent nonelastic deformations, which take place in the environment of the defects, a collective phenomenon. We have seen that certain events known to appear in stress-strain computer experiments on amorphous solids or on ideal lattices take place also in our crystals with defects during stress relaxation. Studying stress-strain behavior of amorphous solids, Vitek, Egami, and collaborators[53–55,15] have *defined* structural defects as configurations of several neighboring atoms that are *collectively* subjected to high atomic-level stress values. Similarly, uniaxially stretched ideal solids[13] seem to show localized collective behavior leading to void formation. In the beginning of this paper we pointed out experimental evidence that stress relaxation curves for different kinds of materials exhibit common features. We intend to find out whether simulations of stress relaxation in molecular chain systems will exhibit features reported above.

ACKNOWLEDGMENTS

Dr. Slawomir Blonski and Miroslaw Latka have participated in programming and in simulation runs. We appreciate discussions with Dr. Franz Fujara, Johannes Gutenberg University, Mainz; Dr. Anatoly Y. Goldman, University of North Texas; Professor Georg Hinrichsen, Polymer Physics, Technical University of Berlin; Dr. Zenon Joffe, Borg-Warner S.A., Villers-Saint-Sepulcre; Professor Robert Kosfeld, Physical Chemistry, University of Duisburg; and Dr. Nikolai N. Medvedev, previously at the University of North Texas and now at the Institute of Chemical Kinetics and Combustion, Novosibirsk.

[1] J. D. Ferry, *Viscoelastic Properties of Polymers,* 3rd ed. (Wiley, New York, 1980).
[2] J. J. Aklonis and W. J. MacKnight, *Introduction to Polymer Viscoelasticity,* 2nd ed. (Wiley, New York, 1983).
[3] J. Kubát, Nature (London) **204**, 378 (1965).
[4] J. Kubát and L.-Å. Nilsson, Mater. Sci. Eng. **52**, 223 (1982).
[5] J. Kubát and M. Rigdahl, in *Failure of Plastics,* edited by W. Brostow and R. D. Corneliussen (Hanser, New York, 1986), Chap. 4.
[6] J. Kubát and M. Rigdahl, Mater. Sci. Eng. **24**, 223 (1976).
[7] L. Bohlin and J. Kubát, Solid State Commun. **20**, 211 (1976).
[8] Ch. Högfors, J. Kubát, and M. Rigdahl, Phys. Status Solidi B **107**, 147 (1981).
[9] J. Kubát, L.-Å. Nilsson, and W. Rychwalski, Res. Mechanica **5**, 309 (1982).
[10] J. Kubát, Phys. Status Solidi B **111**, 599 (1982).
[11] K. Binder, in *The Monte Carlo Method in Condensed Matter Physics,* edited by K. Binder (Springer, Berlin, 1991), Chap. 1.
[12] W. Brostow, R. Cook, and J. Kubát, in *Integral Methods in Science and Engineering–90,* edited by A. Hadji-Sheikh (Hemisphere, Washington, D.C., 1991), p. 24.
[13] Zh.-G. Wang, U. Landman, R. L. Blumberg Selinger, and W. M. Gelbart, Phys. Rev. B **44**, 378 (1991).
[14] D. Deng, A. S. Argon, and S. Yip, Philos. Trans. R. Soc. London, Ser. A **329**, 613 (1989).
[15] D. Srolowitz, V. Vitek, and T. Egami, Acta Metall. **31**, 335 (1983).
[16] W. Brostow and D. P. Turner, J. Rheol. **30**, 767 (1986).
[17] S. Blonski and W. Brostow, J. Chem. Phys. **95**, 2890 (1991).
[18] J. C. M. Li, Can. J. Phys. **45**, 493 (1967).
[19] J. Kubát, M. Rigdahl, and R. Seldén, J. Appl. Polymer Sci. **20**, 2799 (1976).
[20] J. Kubát, R. Sélden, and M. Rigdahl, J. Appl. Polymer Sci. **22**, 1715 (1976).
[21] J. Kubát, Makromol. Chem. Suppl. **3**, 233 (1979).
[22] C. Högfors, J. Kubát, and M. Rigdahl, Rheol. Acta, **24**, 250 (1985).
[23] C. H. Bennet, in *Diffusion in Solids: Recent Developments,* edited by A. S. Novick and J. J. Burton (Academic, New York, 1975).
[24] G. H. Gilmer, Science **208**, 355 (1980).
[25] F. F. Abraham, Phys. Rev. Lett. **44**, 463 (1980).
[26] F. F. Abraham, Phys. Rep. **80**, 339 (1981).
[27] F. F. Abraham, Phys. Rev. Lett. **50**, 978 (1983).
[28] F. F. Abraham, Phys. Rev. B **28**, 7338 (1983).
[29] F. F. Abraham, W. E. Rudge, D. J. Auerbach, and S. W. Koch, Phys. Rev. Lett. **52**, 445 (1984).
[30] G. Mie, Ann. Phys. IV. Folge **11**, 657 (1903).
[31] M. P. Allen and D. J. Tildesley, *Computer Simulation of Liquids* (Clarendon, Oxford, 1987).
[32] H. J. C. Berendsen, J. P. M. Postma, W. F. van Gunsteren, A. DiNola, and J. R. Haak, J. Chem. Phys. **81**, 3684 (1984).
[33] D. Brown and J. H. R. Clarke, Macromolecules **24**, 2075 (1991).
[34] A. J. C. Ladd, in *Computer Modelling of Fluids, Polymers and Solids,* edited by C. R. A. Catlow, S. C. Parker, and M. P. Allen (Kluwer, Dordrecht, 1990).
[35] W. Brostow, Mater. Chem. Phys. **13**, 47 (1985).
[36] W. Brostow, Makromol. Chem. Symp. **41**, 119 (1991).
[37] P. J. Flory, J. Am. Chem. Soc. **87**, 1833 (1965).
[38] P. J. Flory, Discuss. Faraday Soc. **49**, 7 (1970).
[39] G. Kanig, Kolloid Z. **190**, 1 (1963).
[40] Z. Roszkowski, Mater. Chem. Phys. **6**, 455 (1981).
[41] W. Brostow, in *Integration of Fundamental Polymer Science and Technology–2,* edited by P. J. Lemstra and L. A. Kleintiens (Elsevier, London, 1988), p. 139.
[42] F. Fujara and W. Petry, Europhys. Lett. **4**, 921 (1987).
[43] W. Brostow, Polymer **21**, 1410 (1980).
[44] D. Deng, A. S. Argon, and S. Yip, Philos. Trans. R. Soc. London, Ser. A **329**, 549 (1989).
[45] H. C. Andersen, J. Chem. Phys. **72**, 2384 (1980).
[46] M. Parrinello and A. Rahman, Phys. Rev. Lett. **45**, 1196 (1980).
[47] W. Brostow, in *Failure of Plastics,* edited by W. Brostow and R. D. Corneliussen (Hanser, New York, 1986), Chap. 10.
[48] D. Lazarus and N. H. Nachtrieb, *Solids under Pressure* (McGraw-Hill, New York, 1963).
[49] N. H. Nachtrieb and C. Coston, *Physics of High Pressures* (Academic, New York, 1965).
[50] S. Mrowec, *Defects and Diffusion in Solids* (Elsevier, Amsterdam, 1980).
[51] W. Brostow, *Science of Materials* (Wiley, New York, 1979); W. Brostow, *Einstieg in die moderne Werkstoffwissenschaft* (Hanser, München, 1985).

[52]N. N. Medvedev, A. Geiger, and W. Brostow, J. Chem. Phys. **93**, 8337 (1990).
[53]T. Egami, K. Maeda, and V. Vitek, Philos. Mag. A **41**, 883 (1980).
[54]D. Srolovitz, K. Maeda, V. Vitek, and T. Egami, Philos. Mag. A **44**, 643 (1981).
[55]D. Srolovitz, T. Egami, and V. Vitek, Phys. Rev. B **24**, 6936 (1981).